Finite Amplitude Effects on Deep Planetary Circulation over Topography*

NELSON G. HOGG

Woods Hole Oceanographic Institution, Woods Hole, Massachusetts

(Manuscript received 1 August 1988, in final form 8 May 1989)

ABSTRACT

Steady flow over large-scale bathymetric changes of a uniform zonal current in a two-layer fluid is studied under the assumptions that it is geostrophic, that relative vorticity can be ignored, that variations in the planetary vorticity are important and that the upper layer is infinitely thick. This is an extension of the analytic work by Rhines to situations in which the interface can have finite deformations. As concluded by Rhines, both from a small amplitude theory and from numerical integration of the time-dependent initial value problem, there are several features of the resulting solutions that bear close resemblance to the classical channel hydraulics phenomenon. These include the downward (upward) dip of the interface when the flow is subcritical (supercritical) with respect to the long Rossby wave phase speed and the formation of sharp frontal regions downstream of the topography. With respect to the latter it is shown in this steady state analysis that the front arises, not from a hydraulic effect in the conventional sense, but from the intersection of characteristics carrying conflicting information from different parts of the boundary. Concomitant with caustic formation is an induced change in upstream conditions. The Froude number dependence is determined. For the small Froude numbers expected of the midocean deep circulation only very large topographic features such as the mid-Atlantic Ridge can be expected to induce a caustic.

1. Introduction

The classical model of the deep circulation by Stommel and Arons (1960a,b) is driven by a prescribed flux across a horizontal interface and is contained within a basin whose bottom is flat. Welander (1969) first considered the effects of planetary-scale bathymetry on this model and pointed out the controlling influence of potential vorticity (f/h) isolines. Two recent papers by Rhines (1983, 1989) have explored the response of the planetary scale circulation to similar scale, small amplitude bathymetry in a model which allows the interface to be controlled by the dynamics. No driving is provided across the interface; instead, the upstream flow is specified.

Rhines gives analytic solutions for the two layer, steady problem under the assumption that perturbations to the interface and the bottom are both small and points out some apparent similarities to classical hydraulic control, in particular the inverse dependence of the interface elevation on the difference between the incident flow rate and the long Rossby wave phase speed. He then numerically integrates the planetary geostrophic (i.e., relative vorticity neglected) time-dependent equations for an initial value problem in which the upper layer is infinitely deep. Although the topography is quite small in amplitude (order a few hundred meters) large amplitude distortions of the incident flow result.

This paper extends the analytic work of Rhines to finite amplitude. Using the method of characteristics analytic, steady state solutions are derived for which neither the bottom nor the interface displacements need be small. These solutions reproduce the end states of the numerical integrations reasonably well and demonstrate that the sharp, frontal features found in the model are not related to the hydraulic jumps found in classical hydraulics but are, instead, caustics which occur where characteristics intersect and bring conflicting information from different portions of the boundary. When a caustic forms it also shields part of the domain from characteristics originating at the boundary. Resolution of this dilemma indicates that the topography can influence the upstream state if a caustic forms.

The flow speeds used by Rhines are an order of magnitude larger than might be anticipated for the deep ocean long-term mean away from strong currents such as the Antarctic Circumpolar Current. More gentle flows indicate the need of topographic features extending almost the full depth of the layer in order to induce caustic formation and influence the upstream state.

2. Formulation

Consider the situation sketched in Fig. 1. There are two layers of different density flowing uniformly with

* Contribution Number 6858 from the Woods Hole Oceanographic Institution.

Corresponding author address: Nelson G. Hogg, Woods Hole Oceanographic Institution, Woods Hole, MA 02543.

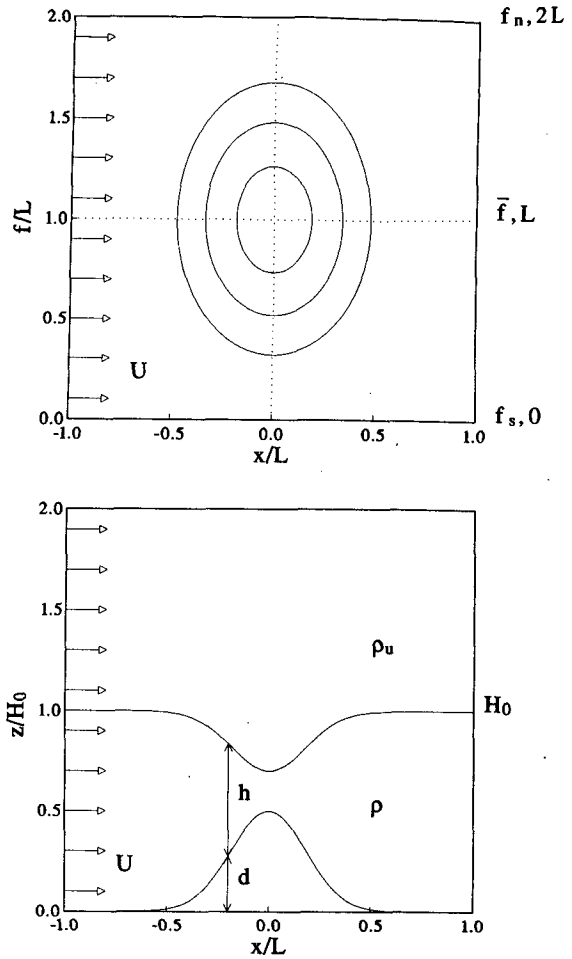

FIG. 1. A schematic drawing of the geometry and flow configuration for two layer flow over Gaussian topography. Figure 1a is the plan view and 1b a side view.

the same speed toward the east and toward a piece of topography which is isolated in the zonal direction and whose height is given by $z = d(x, y)$. The upper layer is infinitely deep so that any effect of the topography is restricted to the lower layer pressure and the interface elevation. The domain is square with sides of length $2L$. It is convenient to take the north-south coordinate as the coriolis parameter $f = \bar{f} + \beta y$ such that the boundaries are at $f_s = \bar{f} - \beta L$ and $f_n = \bar{f} + \beta L$ and $\bar{f}$ is the value of the coriolis parameter at the center latitude. In the analysis below we shall mainly restrict our attention to the special case of an equatorial β-plane in which case $f = \beta y$ making $f_s = 0$ and $f_n = 2\beta L$. We will assume that motions are geostrophic and of sufficiently large scale that relative vorticity can be neglected (i.e., "planetary geostrophic").

From the hydrostatic equation the excess pressure in the lower layer is found to be

$$p = -\int fU dy + g'(d + h) \tag{1}$$

where $g' = g(\rho - \rho_u)/\rho$ is the reduced gravity. Ignoring relative vorticity the potential vorticity equation is

$$\mathbf{u} \cdot \nabla q = 0, \quad q \equiv \frac{f}{h} \tag{2}$$

or, after using geostrophy:

$$\left(U - \frac{g'}{f}(d + h)_y\right) q_x + \frac{g'}{f}(d + h)_x q_y = 0. \tag{3}$$

Using the definition for q the lower layer thickness, $h(x, y)$ can be eliminated from (3) and we obtain

$$\left(U - \frac{g'\beta}{fq} - \frac{g'd_y}{f}\right) q_x + \frac{g'd_x}{f} q_y = 0. \tag{4}$$

This is in characteristic form with the characteristic velocity given by the group velocity, as modified by the bottom slope, plus the mean barotrophic advection.

Scaling the coriolis parameter by $\bar{f}$ and horizontal distance by $\bar{f}/\beta$ for the midlatitude, or βL and L for the equatorial β-plane, the velocity by U and heights by the lower layer thickness on the eastern boundary, H_0, puts equation (4) in the following nondimensional form:

$$\left(\mathrm{Fr} f - \frac{1}{q_0} - d_f\right) q_x + d_x q_y = 0. \tag{5}$$

Because q is conserved along characteristics it has been replaced in the characteristic speed by its value, q_0, at the origin of the characteristic. The nondimensional Froude number:

$$\mathrm{Fr} = \frac{U\bar{f}^2}{g'\beta H_0} \quad \text{or} \quad \mathrm{Fr} = \frac{U\beta L^2}{g' H_0} \tag{6}$$

(midlatitude or equatorial β-plane) is the ratio of the mean advection to the long Rossby wave speed without topography. The eastward zonal flow is opposed to the westward phase propagation of the long Rossby waves, and provided that

$$\mathrm{Fr} f_n^2 < \frac{f_n}{q_0} \leqslant 1 \tag{7}$$

the characteristic velocity will be westward away from the topography and information will originate to the east. We will restrict ourselves to this, subcritical, case although this is not essential. Note that the topographic component of the characteristic speed can cause local reversals and that the y-component induces southward (northward) characteristic speeds to the east (west) of a topographic high.

The slope of a characteristic is then given by

$$\frac{df}{dx} = \frac{d_x}{\mathrm{Fr} f - (1/q_0) - d_f} \tag{8}$$

and this equation can be integrated exactly:

$$d(x, f) = d(x_0, f_0) + \frac{f_0 - f}{q_0} + \frac{\mathrm{Fr}}{2}(f^2 - f_0^2) \tag{9}$$

where (x_0, f_0) are the coordinates of the characteristic at its origin. This equation will form the basis of our analysis. Given the bottom height and potential vorticity at a starting location, $d(x,f)$ at another latitude can be found from Eq. (9) and this inverted to obtain x. The principle difficulty comes in determining the regions of influence of different portions of the boundary.

3. Solution for Gaussian topography

Equation (9) gives the position of a characteristic (x,f) as a function of its initial position and vorticity. In order to invert for (x,f) we need to specify a topographic shape $d(x,f)$ which we will take to be the Gaussian form:

$$d(x,f) = D_0 \exp\left(-\frac{x^2}{X^2} - \frac{(f-1)^2}{Y^2}\right) \quad (10)$$

centered at the midpoint of the domain $(x,f) = (0, 1)$ with X and Y giving decay scales in the zonal and meridional directions. The size of X is unimportant except that we wish $d(x, y)$ to be sufficiently small at the east and west boundaries that it can be neglected there. We will use $X = 0.25$. The value of Y will be varied from $Y = \infty$ appropriate for a meridional ridge to $Y = 0.25$ for an isolated topographic high.

For characteristics beginning at the eastern boundary, $q_0 = f_0$ and Eq. (9) gives f_0 as a cubic function of d and f. This suggests that characteristics originating at different points along the eastern boundary might cross, i.e., for given values of d and f there may be more than one starting latitude f_0. Figure 2a shows the (d,f) relationship for different values of f_0 and, indeed, they do cross for topographic heights above a value which depends on the scaled latitude $\sqrt{\mathrm{Fr}}f$. This is illustrated for a Gaussian ridge ($Y = \infty$) in Fig. 2b. The locus of the points at which characteristics cross is where

$$\frac{\partial d}{\partial f_0} = 0$$

or

$$f = \mathrm{Fr} f_0^3 = \mathrm{Fr} f_0^2 \cdot f_0 < f_0, \quad (11)$$

from Eq. (7). Substitution in Eq. (9) gives

$$d = 1 - \frac{3}{2}(\mathrm{Fr} f^2)^{1/3} + \mathrm{Fr} f^2 \quad (12)$$

for the locus of intersections [taking $d(x_0, f_0) = 0$]. This is the heavy dashed curve in Fig. 2a; topographies which rise above this curve as a function of f so distort the characteristics that they intersect. Such an intersection represents a conflict of information arriving from the eastern boundary and results in the formation of a caustic whose shape is given by Eq. (12).

For the case of a meridional ridge the northern extent of the caustic is determined by the northernmost characteristic originating from the eastern boundary. For those coming from the northern boundary, intersections would result where

$$\frac{\partial d}{\partial x_0} = 0 \quad (13)$$

which can easily be shown to be an impossibility; characteristics from the northern boundary do not intersect one another but can, of course, intersect those from the east. For more confined topography with Y finite the characteristic pattern can be more complex with stagnation points and associated zonal speed reversals. These regimes are defined in the $D_0 - Y^{-1}$ plane in Fig. 3 for two values of Fr, a slightly subcritical value

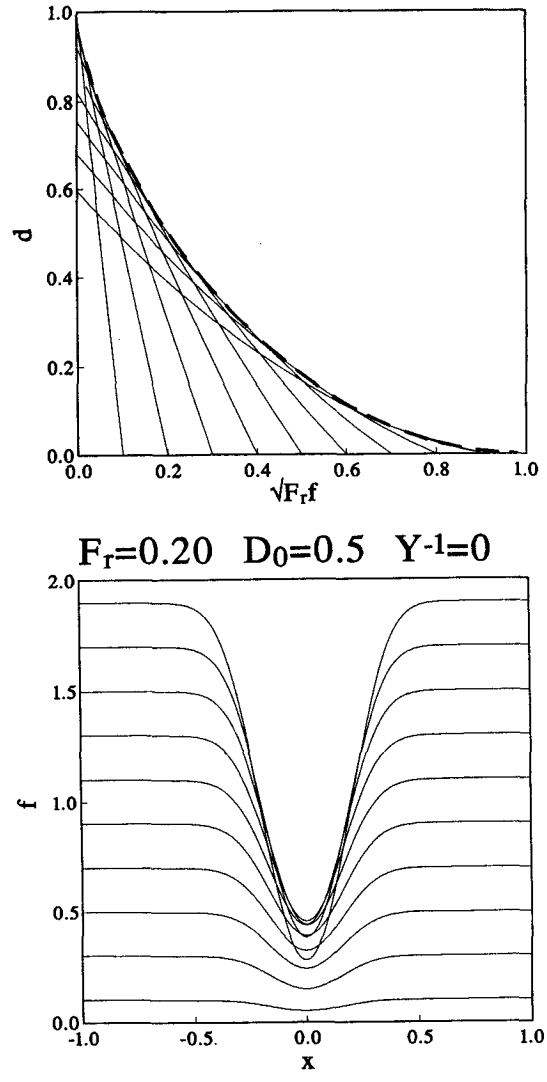

FIG. 2. Trajectories of evenly spaced characteristics emanating from the eastern boundary and being disrupted by a uniform meridional ridge. Panel (a) gives the characteristics treating d as the dependent variable while Panel (b) is in physical space. The heavy dashed curve in Panel (a) is the locus of the points of intersection of the characteristics.

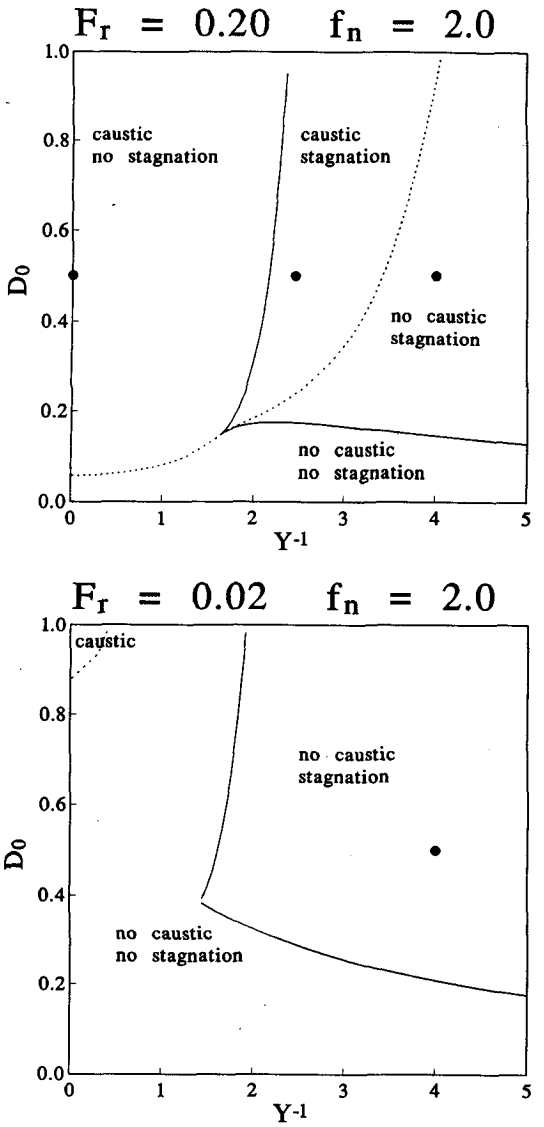

FIG. 3. Regime diagram showing the parameter values needed for caustic and stagnation point formation for (a) Fr = 0.2 and (b) Fr = 0.02.

Fr = 0.2 (putting the critical latitude at 2.24 just north of $f_n = 2$) and a low value Fr = 0.02. The methods for determining the different regime boundaries are outlined in the Appendix.

The curves in Fig. 3 divide the $(D_0 - Y^{-1})$ plane into three or four different regimes depending on the value of Fr. In both cases the solid curve distinguishes where a stagnation point just develops in the interior of the domain. Along the nearly vertical portion the stagnation characteristic originates at the northeast corner and, consequently, depends on there being a northern boundary while along the nearly horizontal portion it originates south of $f = f_n$ and, therefore, is unaffected by the northern boundary. The dotted curve in Fig. 3 identifies the dependence of D_0 on Y^{-1} for which a caustic just forms. There are two connected sections of this curve. The one in the regime with no stagnation point is determined by insisting that the intersection between the caustic equation (12) and the characteristic from the northeast corner occur somewhere along $x = 0$ (i.e., no caustic). When there is a stagnation point, caustic formation is determined by the condition that the stagnation characteristic intersect the caustic along $x = 0$. Thus, there are two curve segments in Fig. 3a (Fr = 0.2) which do not depend on the presence of the northern boundary and two which do. In Fig. 3b (Fr = 0.02) one of these occurs for $D_0 > 1$, which is impermissible if the active fluid layer is to have nonvanishing thickness.

These regimes are illustrated in Fig. 4 by drawing the caustic and the important dividing characteristics for $D_0 = 0.5$ and the various values of Y^{-1} shown by the large dots in Fig. 3. Figures 4a–c are from Fr = 0.2, the slightly subcritical case. When $Y = \infty$ (i.e., a ridge, Fig. 4a) there can be no stagnation point and the caustic begins at the ridge peak and terminates where it is tangent to the characteristic coming from the northeast corner. Another characteristic exists further to the south, which is tangent to the caustic's origin at the ridge crest and this defines a band of latitudes for which information originating from the eastern boundary terminates at the caustic (region B). Characteristics from a portion of the northern boundary to the west of the northeast corner also terminate at the caustic (region C). Finally, there is a characteristic which begins at $(0, f_n)$ and loops south and back on itself. Inside of this closed region E no information from the boundaries can penetrate, and the steady state solution will depend on dissipation (e.g., homogenized potential vorticity).

There is an additional region F for which information is not supplied from the boundaries. This is the area to the northwest bounded by the characteristic from $(0, f_n)$ and the one defining the southern extent of the caustic. Provided that flow remains subcritical, information flow is toward the west and north but has no obvious source. Further discussion of this problem and its resolution will be reserved for the next section.

For somewhat higher $Y^{-1} = \sqrt{6}$ the dividing characteristics are displayed in Fig. 4b. This is in the regime for which a stagnation point with associated closed characteristics forms (Fig. 3a). The termination of the caustic is determined by where it is tangent to the stagnation streamline. The northern boundary now does not play a critical role; all of its characteristics skirt to the north of the stagnation characteristic beginning and ending on $f = f_n$. There is a substantial region south of the stagnation characteristic and to the west of the caustic in which no information from the boundaries can penetrates and for which appeal to some higher order process must be made.

At the yet higher $Y^{-1} = 4$ of Fig. 4c the caustic has vanished and there now exists just the stagnation characteristic which encloses a region which is cutoff from

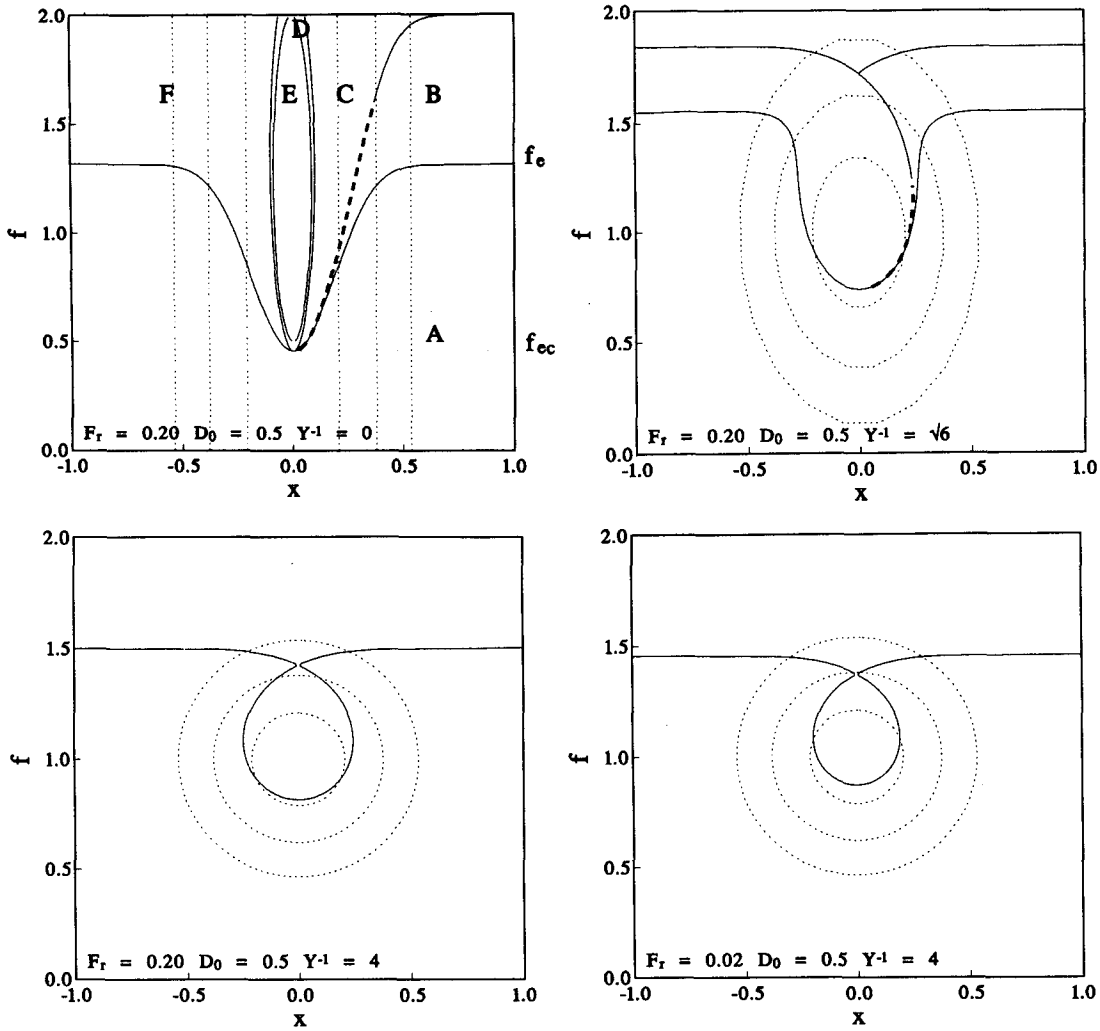

FIG. 4. Critical characteristics which divide the domain into regimes receiving their information from different portions of the boundary. Panels (a–c) are for Fr = 0.2 while (d) is for Fr = 0.02. The finely dashed curves give the topographic contours at 0.01, 0.1, and 0.5 of the maximum height $D_0 = 0.5$. The heavy dashed curve denotes the caustic which forms only in (a) and (b).

the boundaries. Everywhere else characteristics bring information in from either the eastern or northern boundaries. Reducing Fr by an order of magnitude (Fig. 4d) gives a very similar picture. Note, as reference to Fig. 3b will confirm, that patterns at the smaller values of Y^{-1} will be quite different from Fig. 4d but no caustic forms at any value of Y^{-1} for $D_0 = 0.5$.

4. Full solution for a Gaussian ridge

There are a large number of possible flow configurations that depend on the specific choice of parameters; only the boundaries of the most important regimes are shown in Fig. 3. The focus of this paper is the formation of caustics and we shall illustrate this by giving the full solution for a Gaussian ridge ($Y^{-1} = 0$) of height $D_0 = 0.5$ and zonal decay scale $X^{-1} = 4$. Further examples will be given in the next section when we make a direct comparison with the numerical integration of Rhines (1989).

Knowing the boundaries of the regimes from Fig. 4a it is a relatively simple matter to compute the q contours as the potential vorticity is conserved along the characteristics. For equally incremented values of q, characteristics are begun along the eastern and northern boundaries in regions A, B, C, and D and terminated where they end at the particular regime or domain boundary. For area E all characteristics are closed and at steady state with weak dissipation the potential vorticity should be uniform and equal to that of the bounding characteristic (Rhines and Young 1982).

Area F is more problematic. As long as flow there remains subcritical, information cannot penetrate from the boundaries. In addition, it is not possible for fronts or caustics to be downstream (in the characteristic

sense) of the ridge as information then would have to diverge from the caustic rather than converge on it. The only solution to this dilemma seems to be that all characteristics must emanate from the point at the ridge crest where areas A, B and C coincide. Varying q from the value on region F's bounding southern characteristic to that on its bounding eastern characteristic then allows q to vary smoothly throughout except for a singularity at the ridge crest. Equation (9) becomes, in region F:

$$d(x,f) = d(0,f_{ec}) + \frac{f_{ec}-f}{q} + \frac{\mathrm{Fr}}{2}(f^2 - f_{ec}^2) \quad (14)$$

valid in region F with f_{ec} being the latitude at which the caustic begins. With this resolution of the dilemma q contours are displayed in Fig. 5a. The asymmetry caused by the caustic is rather subtle but note that q contours in the northwest asymptote to a higher latitude than they do in the east, which implies an influence upstream by the topography.

With the substitution $q = f/h$ Eqs. (9) and (14) can be written as explicit relations for $d(x,f)$. For example, (14) becomes

$$d(x,f) = d(0,f_{ec}) + \frac{(f_{ec}-f)}{f}h + \frac{\mathrm{Fr}}{2}(f^2 - f_{ec}^2) \quad (15)$$

valid in region F. By now incrementing h and keeping track of regime boundaries contours of constant layer thickness, h, are rather easily constructed. However interface elevation, $\eta = d + h - 1$, is more revealing and this can be determined for each region through substitution into Eqs. (9) and (14). After some rearrangement these become

$$d(x,f) = 1 + \eta - \frac{1}{\sqrt{1 - (2\eta/\mathrm{Fr}f^2)}},$$

in regions A and B;

$$f^2 = f_n^2 + \frac{2\eta}{\mathrm{Fr}}, \quad \text{in regions C and D;}$$

$$d(x,f) = \frac{f}{f_{ec}}d(0,f_{ec}) + \left(1 - \frac{f}{f_{ec}}\right)(1+\eta) + \frac{\mathrm{Fr}}{2}(f^2 - f_{ec}^2), \quad \text{in region F.} \quad (16)$$

The contours of η are displayed in Fig. 5b. Upstream influence is again evident in region F.

From equation (2) it can be seen that the Jacobian of the transport streamfunction, $d\mathbf{u} \equiv \mathbf{k} \times \nabla\psi$, and the potential vorticity vanishes. Therefore, lines of constant ψ coincide with lines of constant q and will resemble Fig. 5a. However, the $q - \psi$ relationship is nonlinear and equally spaced q contours will not necessarily be

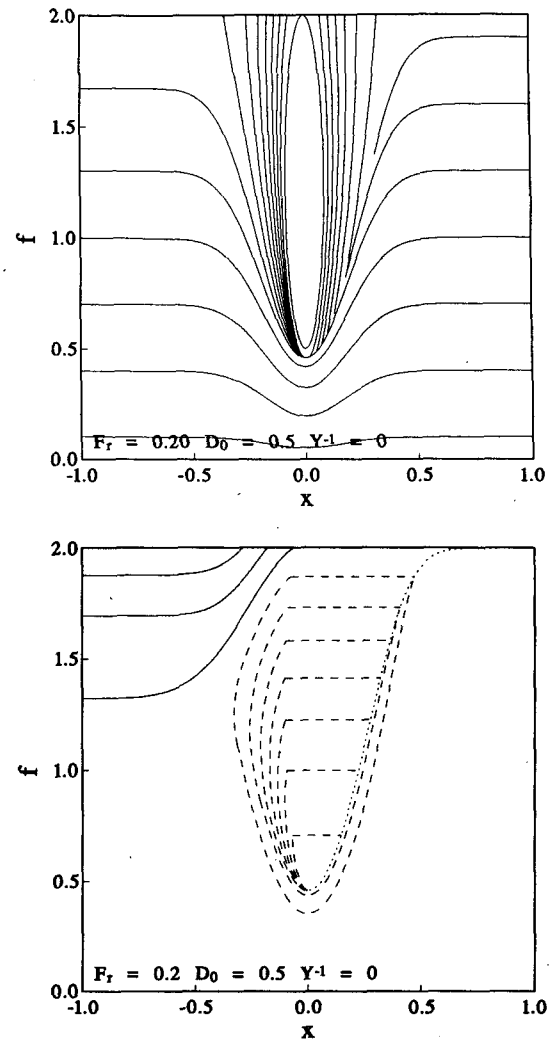

FIG. 5. Contours of (a) potential vorticity and (b) interface elevation for flow over a uniform ridge. The contour interval in (a) is 0.3 units and in (b) it is 0.05 units with dashed contours being negative. Contours increment monotonically.

equally spaced ψ contours. The relationship between the two can be evaluated at the boundaries. A nondimensional version of Eq. (1) for pressure is

$$p = \frac{f^2}{2} + \frac{1}{\mathrm{Fr}}(d+h) \quad (17)$$

On the eastern boundary where $h = 1$ and $d = 0$, this gives for the streamfunction:

$$\psi = -f. \quad (18)$$

Here ψ and q are linearly related. On the northern boundary in regions C and D (Fig. 4a) the normal velocity vanishes giving

$$\psi = -f_n \quad (19)$$

after matching with (18) at $f = f_n$.

Region F is more difficult as the conditions along the boundary are set by the characteristics flowing from the termination point of the caustic at the ridge crest. The streamfunction along the western wall north of $f = f_e$ can be found by integrating:

$$\psi_f = \frac{h}{f} p_f = \frac{h}{f}\left(-f + \frac{h_f}{\mathrm{Fr}}\right). \qquad (20)$$

This can be done analytically but is not reproduced here. In a similar fashion ψ can be determined along the northern boundary where the normal velocity component no longer vanishes and

$$\psi_x = \frac{h}{f} p_x = \frac{1}{f\mathrm{Fr}}\left(\frac{\partial}{\partial x}\frac{h^2}{2} + h d_x\right). \qquad (21)$$

Finally, evaluating ψ at the eastern edge of region F does not give the value $-f_n$ found at the beginning of this characteristic to the east of the ridge crest [Eq. (19)]. In fact, there is more fluid flowing in through the western and northern boundaries than is flowing out across the eastern boundary.

This excess is more easily established by integration of (21) across the latitude $f = f_e$. After considerable algebra, the streamfunction of the characteristic bounding the eastern side of region F can be simplified to

$$\psi = -f_e + \frac{\mathrm{Fr}}{8}(f_n^2 - f_e^2)\left(\frac{f_n^2}{f_e^2} - 5\right). \qquad (22)$$

The ratio of the excess of mass inflow over total outflow is shown in Fig. 6. It vanishes for topographic heights smaller than that required for caustic formation. At a height $D_0 \approx 0.5$ regions D and E coincide, and for larger heights the characteristic coming from $(0, f_n)$ intersects the caustic at $x > 0$ thereby changing the characteristic geometry.

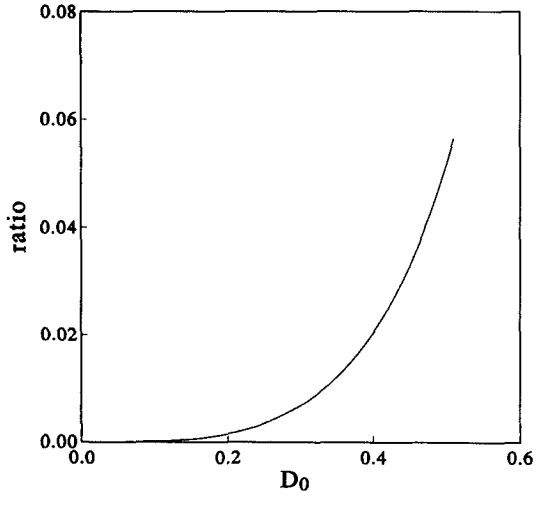

FIG. 6. The ratio of the difference between the mass inflow and outflow to the outflow versus ridge height D_0.

The lack of mass conservation in this model is troublesome. It undoubtedly arises from the method in which the potential vorticity has been determined in region F. This is admittedly ad hoc but we have been unable to find another method that does not produce fronts. We presume that the mass inflow excess must be absorbed by the singularity where the caustic begins at the ridge crest.

5. Application to Rhines's numerical experiments

Rhines (1989) derives a single, nonlinear, partial differential equation for the interface elevation for the time-dependent initial value problem with small diffusion. He uses periodic conditions on the meridional boundaries and conditions of no normal flow and no interface flux on the zonal boundaries. His experiments cover a range of subcritical, supercritical and mixed upstream states. We shall focus on the subcritical cases displayed in his Figs. 3–6 and reproduced here as Figs. 7a and 8a. Both are in 2500 km × 2500 km domains on the β-plane with $\beta = 2 \times 10^{-11}$ m s^{-1}, $f = 7.3 \times 10^{-5}$ s^{-1} and $g' = .005$ m s^{-2}. Both have Gaussian shaped topographies centered in the domain with maximum elevations of 300 m in a total layer depth of 2000 m and both have uniform incident upstream flow of $U = 0.02$ m s^{-1}. The only differences are in the horizontal topographic scales: the more confined one has $X = 300$ km and $Y = 600$ km while the other has scales larger by a factor of 10. The nondimensional parameters take on the values Fr = 0.533, $f_n = 1.342$, $f_s = 2 - f_n = 0.658$, $D_0 = 0.15$ and $X^{-1} = 12.2$, $Y^{-1} = 6.1$ or $X^{-1} = 1.22$, $Y^{-1} = 0.61$ depending on the experiment.

For flow over the more confined bump the potential vorticity contours are shown in Fig. 7a at numerical steady state (i.e., at a point where any noticeable changes were no longer occurring). The most prominent feature is the north–south asymmetry to the distortion introduced by the bump with flow being accelerated to the south and decelerated to the north. Less noticeable is an east–west asymmetry with a relatively sharper gradient in q downstream and an associated drawdown of the q contours to the north. Contours over the bump are closed. In Fig. 7b we show the analogue of Fig. 3—the critical dividing characteristics and curves which separate regimes with different potential vorticity source distributions in the steady state model. These are now computed with the actual distributions along the boundary and take into account the possibly finite height of the topography there. The topography is high enough to form a caustic, which extends almost all the way to the northern boundary and closely coincides with the sharp gradient region to the east of the bump crest in Fig. 7a. Contours of constant q are given by Fig. 7c and resemble those of the numerical integration. Major differences include our inability to compute the contours where they are closed

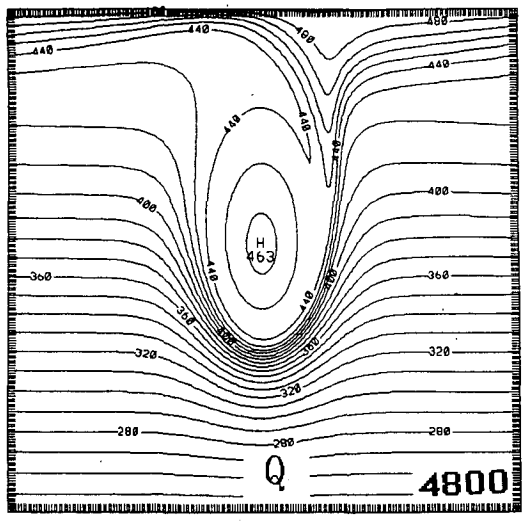

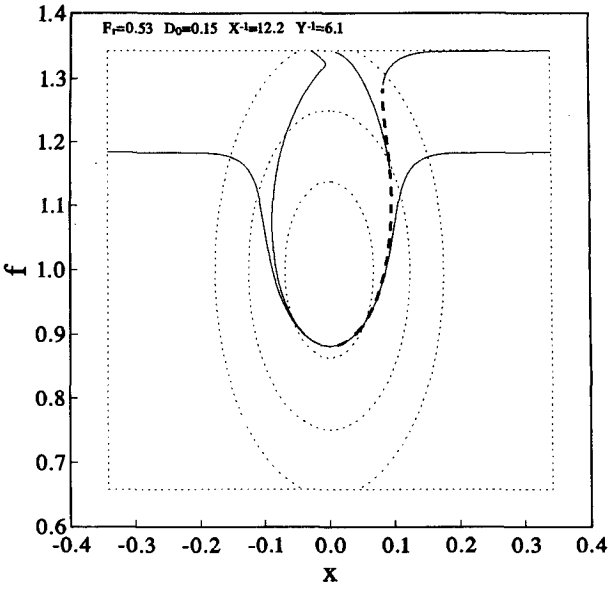

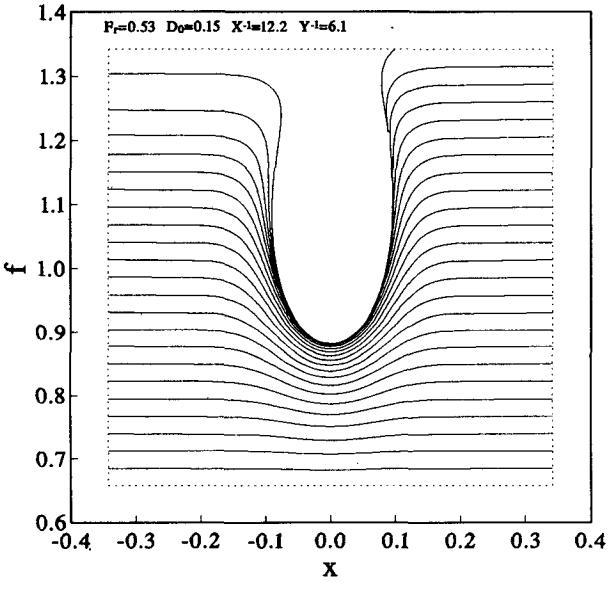

FIG. 7. A comparison between the (a) end state of Rhines's (1989) numerical integration of the time dependent initial value problem with (b) the predicted critical steady state characteristics and (c) the predicted contours of constant potential vorticity. The contour interval in (c) is chosen to be that of (a). This is a confined Gaussian hill with $X^{-1} = 12.2$ and $Y^{-1} = 6.1$. Bathymetric contours are at 0.01, 0.1 and 0.5 of the peak elevation.

and our use of nonperiodic boundary conditions. Those characteristics that originate along the northern boundary have almost uniform values of q_0 and explain the area of weak q gradients to the north of the caustic.

The broader bump is displayed in Fig. 8 in the same sequence as Fig. 7. This is in a similar regime to that of Fig. 7 and results in a similar pattern, which is more spread out. Because the bump has appreciable height at the meridional boundaries the recycling boundary conditions substantially change the eastern boundary condition north of about the midlatitude and causes the caustic to be displayed somewhat to the south of the point that is predicted in Fig. 7b. Presumably better agreement could be reached by iterating the eastern boundary condition using some fraction of the predicted value along the west.

6. Discussion and conclusion

As was pointed out by Rhines (1989) there are several features of this topographic problem reminiscent of more classical channel hydraulics. The appearance of sharp gradients downstream of the bump crest, here interpreted as a caustic, has some visual similarity to the formation of jumps downstream of control (choke) points. If the depths are renormalized by a further factor of $(\mathrm{Fr} f^2)^{1/3}$ Eq. (16) for interface displacement can be rewritten as

$$h^* = d^* + \frac{1}{2d^{*2}}$$

which is precisely the cubic form found in channel hydraulics (e.g., see Gill 1977). This apparent equivalence between the two situations is deceptive. In the

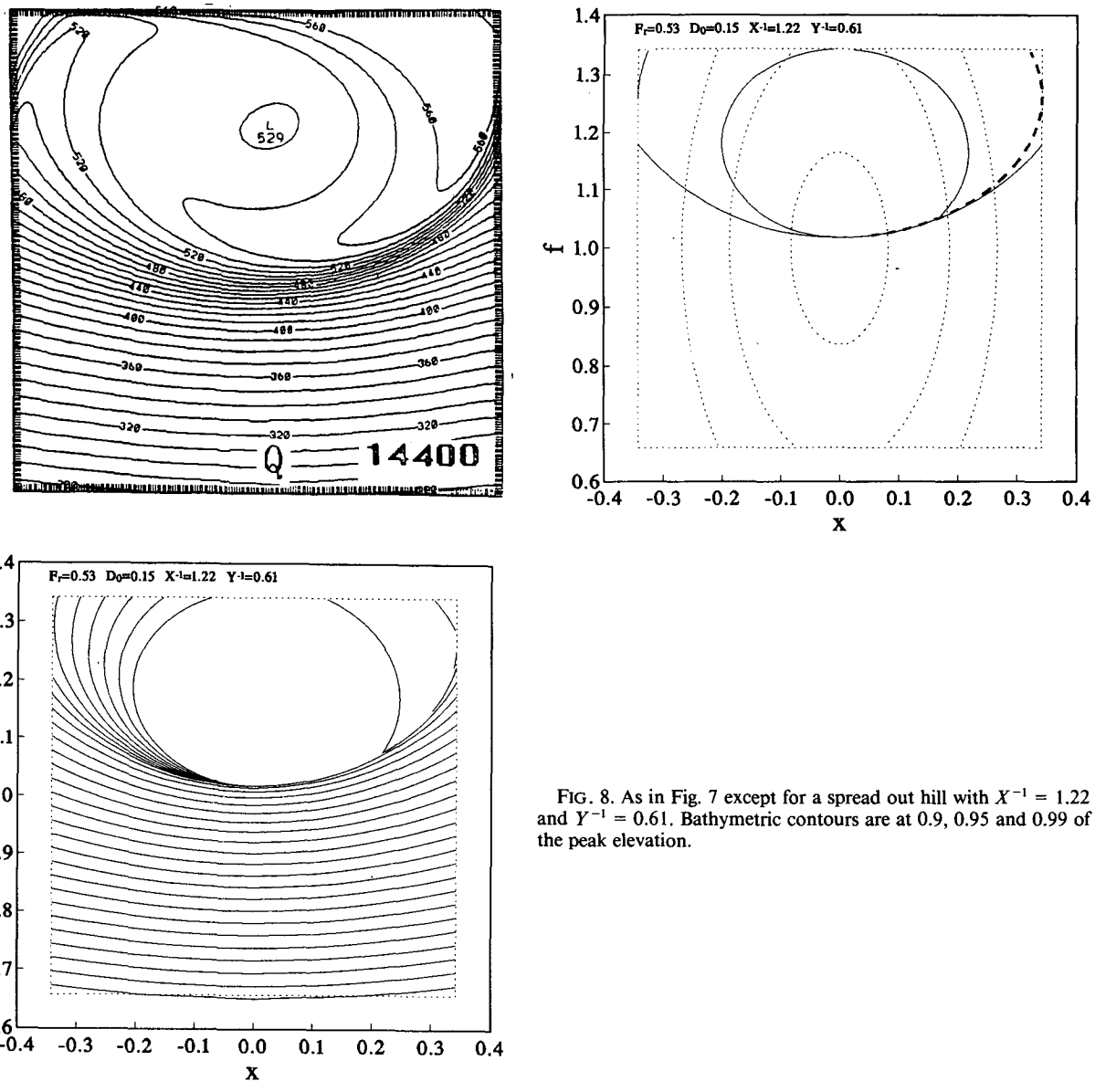

FIG. 8. As in Fig. 7 except for a spread out hill with $X^{-1} = 1.22$ and $Y^{-1} = 0.61$. Bathymetric contours are at 0.9, 0.95 and 0.99 of the peak elevation.

channel flow problem a continuous solution is obtained by insisting that the control point occur at the extremum of the cubic relation ($h^* = 1.0$, $d^* = 1.5$) which is also where the local Froude number is unity. For the planetary problem, in the "unstarred" quantities, this occurs at $h = (\mathrm{Fr} f^2)^{1/3}$ whereas it can be shown that the local Froude number is unity when $h = \mathrm{Fr} f^2$, which is greater than $(\mathrm{Fr} f^2)^{1/3}$ and is, instead, the point at which a caustic forms.

Besides different dynamics another important distinction between the planetary flow problem considered herein is that it is fundamentally two-dimensional. The variation of the coriolis parameter makes the phase speed of the long Rossby waves a function of latitude so that even for a uniform ridge in a uniform flow the response is two-dimensional.

Our results, particularly as regards caustic formation, are strongly dependent on the upstream Froude number as defined by Eq. (6). Rhines uses parameter values that lead to near critical values of $\mathrm{Fr} f_n^2$. In particular, he takes flow speeds on the order of a few centimeters per second, intended to be typical of the deep Antarctic Circumpolar Current. Away from such strong flows the subthermocline deep interior is believed to be much weaker if driven by the Stommel and Arons (1960a,b) process. Flow speeds of a few millimeters per second reduces the Froude number by an order of magnitude, and reference to Fig. 2a will show that ridge heights on the order of the layer depth (e.g., mid-ocean ridges) are required to produce caustic features in the flow.

This model has particularly simple physics being barotropic upstream and having an infinitely thick up-

per layer. It would be of some interest to extend these results to more realistic regimes.

Acknowledgments. This work has been supported by Grant OCE86-08258 from the National Science Foundation and Contrast N00014-85-C-0001, NR 083-004 with the Office of Naval Research. Comments from Roger Samelson and Peter Rhines are appreciated.

APPENDIX

Regime Boundaries

For characteristics originating at the eastern boundary where $q_0 = f_0$ and $d = 0$, Eq. (9) become

$$d(x, f) = 1 - \frac{f}{f_0} + \frac{\mathrm{Fr}}{2}(f^2 - f_0^2) \quad , \qquad \text{(A1)}$$

The caustic condition (11) gives the shape of the caustic as in Eq. (12). If we take $f_0 = f_n$ then we determine the northeasterly extent of the caustic. If in addition, we take $x = 0$ such that

$$d(0, \mathrm{Fr} f_0^3) = D_0 \exp(-(\mathrm{Fr} f_0^3 - 1)^2/Y)$$

$$= 1 - \frac{3}{2}\mathrm{Fr} f_0^2 + \frac{1}{2}\mathrm{Fr}^3 f_0^6 \qquad \text{(A2)}$$

and $f_0 = f_n$ we have determined the $D_0 - Y^{-1}$ relationship for caustic formation, given Fr and f_n. This is the dotted line beginning on the D_0 axis of Figs. 3a and 3b.

A characteristic coming from the northeast corner will just stagnate when

$$\frac{\partial f_0}{\partial f} = 0 \qquad \text{(A3)}$$

along $x = 0$. Applying this condition to (A1) we get

$$-\frac{2(f-1)d(0,f)}{Y^2} = -\frac{1}{f_0} + \mathrm{Fr} f \qquad \text{(A4)}$$

using the Gaussian topographic form. With $x = 0$ and $f_0 = f_n$ in (A1), $d(0, f)$ can be substituted in (A4) giving a cubic equation for f. Solving this for given Y then allows D_0 to be calculated from (A1) and this gives the nearly horizontal solid curve of Fig. 3.

Neither of these characteristics need originate at the northeast corner. If the critical stagnation characteristic comes from $f_0 < f_n$ then we must determine f_0 as well, which comes from the additional condition

$$\frac{\partial^2 f_0}{\partial f^2} = 0 \qquad \text{(A5)}$$

or

$$\frac{2}{Y^2}\left(\frac{2(f-1)^2}{Y^2} - 1\right) d(0, f) = r \qquad \text{(A6)}$$

specifying that, in addition to this being the stagnation characteristic, it is also the only one that stagnates. Conditions (A1) (with $x = 0$), (A4) and (A6) are solved for D_0 versus Y^{-1} using a nonlinear rootfinder (Press et al. 1988). This gives the upright portion of the solid curve in Fig. 3.

Finally, when a stagnation point does develop the condition for caustic formation must be modified. The termination of the caustic is now determined by where it intersects the stagnation characteristic, so we add to (A1) (with $x = 0$) and (A2) condition (A4). Again the root solver must be used and we obtain the dotted curve in the stagnation region of Fig. 3a.

REFERENCES

Gill, A. E., 1977: The hydraulics of rotating-channel flow. *J. Fluid Mech.*, **80**, 641–671.

Press, W. H., B. P. Flannery, S. A. Teukolsky and W. T. Vetterling, 1988: *Numerical Recipes in C.* Cambridge University Press, 735 pp.

Rhines, P. B., 1983: Lectures in geophysical fluid dynamics. *Lectures in Applied Mathematics, Vol. 20,* American Mathematics Society, 3–58.

——, 1989: Deep planetary circulation and topography: Simple models of midocean flows. *J. Phys. Oceanogr.*, in press.

——, and W. R. Young, 1982: Homogenization of potential vorticity in planetary gyres. *J. Fluid Mech.*, **122**, 347–367.

Stommel, H., and A. B. Arons, 1960a: On the abyssal circulation of the world ocean–I: Stationary planetary flow patterns on a sphere. *Deep-Sea Res.*, **6**, 140–154.

——, and ——, 1960b: On the abyssal circulation of the world ocean–II: An idealized model of the circulation pattern and amplitude in oceanic basins. *Deep-Sea Res.*, **6**, 217–233.

Welander, P., 1969: Effects of planetary topography on the deep-sea circulation. *Deep-Sea Res.*, **16**(Suppl.), 369–391.